Improved Finite-Difference Formulation in Frequency Domain for Three-Dimensional Scattering Problems

Klaus Beilenhoff, *Member, IEEE*, Wolfgang Heinrich, *Member, IEEE*, and Hans L. Hartnagel, *Senior Member, IEEE*

Abstract—**The finite-difference method in the frequency domain is a powerful tool for analyzing arbitrarily shaped transmission-line discontinuities and junctions. In this paper, an improved formulation based on Maxwell's equations in integral form is presented. It corresponds to the Helmholtz equation and reduces the numerical efforts in solving the large linear equation system considerably. The method is verified by comparison to previous work on microstrip.**

I. Introduction

THE DESIGN of monolithic microwave integrated circuits (MMIC) requires reliable modeling tools [1]. Because it is impossible to tune circuit performance after fabrication, a very precise *a priori* knowledge of passive and active elements is mandatory if time consuming and costly redesign cycles are to be avoided.

High-frequency devices (e.g., transmission-line connections, couplers, filters) are usually described in terms of their scattering matrix. Several methods are known for determining the scattering behaviour of passive structures using a field-theoretical approach. The mode-matching method [2] e.g., gives very accurate results but it can only be applied to certain geometries. The spectral domain method, on the other hand, leads to very efficient algorithms (e.g., [3]). The main disadvantages of this method are, however, that only planar structures can be analyzed and that metallization thicknesses larger than zero cause problems. During the last five years, the time domain methods became more and more important, especially the finite-difference method (FDTD) [4]. Its principal advantage is that only one step is required for the calculation of a broad range of frequencies. On the other hand, the *S*-parameters represent basically frequency-domain quantities. This inconsistency causes, for instance, that one can allow for only one propagating mode on each longitudinally homogeneous transmission line attached to the discontinuity under investigation. Hence, mode conversion cannot be considered.

In this paper the finite-difference method in the frequency domain is employed. There are several advantages in using this method. First, it allows one to simulate the electric and magnetic field of nearly arbitarily shaped structures. The materials may have a frequency dependent complex permittivity and permeability. Further, this method has been employed successfully in connection with cavity resonator problems [5]. One additional reason for using the frequency domain is the compatibility with the mode concept and thus the straightforward derivation of the scattering matrix.

In the following, a short description of the finite-difference method in the frequency domain is given and the improved formulation is introduced. To show the reduction in numerical efforts, the computational time of the program for the new formulation is compared with the standard version. Finally, a check against other methods shows the accuracy of our approach.

Manuscript received May 13, 1991; revised October 9, 1991.

The authors are with the Institut fur Hochfrequenztechnik, Technische Hochschule Darmstadt, Merckstrasse 25, D-6100 Darmstadt, Germany.

IEEE Log Number 9105443.

II. The FD-Method in the Frequency Domain

Generally speaking, a boundary value problem is treated here. In its simplest case, the bounded region is a rectangular box. It encloses the line discontinuity and the attached longitudinally homogeneous transmission lines representing the ports. This large box is subdivided into elementary cells by a three-dimensional nonequidistant Cartesian grid. The electric field components are defined at the central points of the corresponding cell edges (see Fig. 1). Therefore, this mesh is called the electric field mesh. Each cell is filled with an isotropic medium described by its permittivity and permeability. Hence, a change in material properties can only be located at the surfaces of elementary cells. In our case, only lossless materials are taken into consideration. Therefore, we assume ϵ_r and μ_r to be real. The magnetic field components are positioned at the central point of each cell surface with a direction perpendicular to that surface. Thus, a second mesh is created which is called the dual grid or the magnetic field mesh. Fig. 1 shows both meshes for a single elementary cell.

The Maxwell equations in integral form for lossless and isotropic materials are given by (1) and (2). Since we are considering the frequency domain, a harmonic time dependence ($e^{j\omega t}$) is assumed, which is not printed in the following:

$$\oint_C \frac{\vec{B}}{\mu} d\vec{s} = \int_A (j\omega\epsilon\vec{E})\, d\vec{A} \tag{1}$$

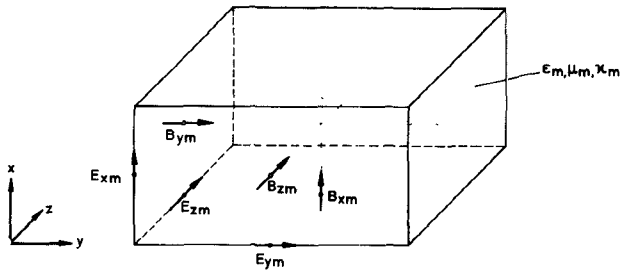

Fig. 1. Field quantities related to an elementary cell.

$$\oint_C \vec{E}\, d\vec{s} = \int_A (-j\omega \vec{B})\, d\vec{A}. \tag{2}$$

The discretization of the analytical equations can be done by the following transformation:

$$\int_{-s_m/2}^{s_m/2} \vec{f}\, d\vec{s} \rightarrow s_m f_m \tag{3}$$

$$\int_{-s_m/2}^{s_m/2} \int_{-t_m/2}^{t_m/2} \vec{f}\, d\vec{A} \rightarrow s_m t_m f_m. \tag{4}$$

For each cell the line integral of a tangential vector can be approximated by multiplying the value at the central point of the corresponding boundary with the line length. In the same way, the surface integral is represented by the multiplication of the value in the center of the surface with the surface area (see Appendix I). One derives a discretized form of Maxwell equations that can be written in matrix notation (see Weiland [6]):

$$\boldsymbol{A}^T \boldsymbol{D}_{s/\mu} \vec{b} = j\omega \epsilon_0 \mu_0 \boldsymbol{D}_{A\epsilon} \vec{e} \tag{5}$$

$$\boldsymbol{A}\boldsymbol{D}_s \vec{e} = -j\omega \boldsymbol{D}_A \vec{b} \tag{6}$$

$\vec{e}$ and $\vec{b}$ are the vectors containing the electric and magnetic fields of the cells, respectively. The boldfaced typed operators denote matrices. $\boldsymbol{A}$ is defined as the operator of the corresponding line integral (see Appendix II). Each coefficient of $\boldsymbol{A}$ is unity or zero, corresponding to the use of the field component for the Maxwell equation of node m. Therefore, $\boldsymbol{A}$ is a canonical matrix and does not involve any information on dimensions or materials of the structure. For field components placed tangential to or inside a metallization, all elements in the corresponding matrix line and row are equal to zero. The abbreviation $\boldsymbol{D}$ refers to diagonal matrices. The index indicates which quantities form the elements of the main diagonal. These matrices contain the information on dimension and material for the specified structure and mesh (see Appendix II). Equations (5) and (6) can be combined to (7) by substituting the magnetic field components:

$$\boldsymbol{A}^T \boldsymbol{D}_{s/\mu} \boldsymbol{D}_A^{-1} \boldsymbol{A} \boldsymbol{D}_s \vec{e} = \underbrace{\omega^2 \epsilon_0 \mu_0}_{k_0^2} \boldsymbol{D}_{A\epsilon} \vec{e}. \tag{7}$$

This formulation corresponds to the analytical expression of $\nabla \times \nabla \times \vec{E} = k_0^2 \vec{E}$. It describes the electromagnetic field inside the enclosure containing the structure under consideration. If no sources exist on the boundaries of the enclosure, (7) represents an eigenvalue problem with the eigenvalues $k_{0\text{res}}$ being resonant frequencies of the cavity. Because we are interested in the scattering matrix, however, waves propagate through the ports and thus we have to assume suitable sources on the boundaries. Hence, the homogeneous system of linear equations (7) turns into an inhomogeneous one (8):

$$(\boldsymbol{A}^T \boldsymbol{D}_{s/\mu} \boldsymbol{D}_A^{-1} \boldsymbol{A} \boldsymbol{D}_s - k_0^2 \boldsymbol{D}_{A\epsilon})\, \vec{e} = \vec{r}. \tag{8}$$

The right-hand side $\vec{r}$ represents the sources which are defined as the sum over all transversal electric fields of the modes propagating on the transmission lines at the ports. The matrix $\boldsymbol{D}_{A\epsilon}$ contains only elements larger than zero. Hence, multiplying $\boldsymbol{D}_{A\epsilon}^{-1}$ from the left-hand side does not change the solution and one has

$$(\boldsymbol{D}_{A\epsilon}^{-1} \boldsymbol{A}^T \boldsymbol{D}_{s/\mu} \boldsymbol{D}_A^{-1} \boldsymbol{A} \boldsymbol{D}_s - k_0^2 \boldsymbol{I})\, \vec{e} = \boldsymbol{D}_{A\epsilon}^{-1} \vec{r} \quad \text{or}$$

$$(\boldsymbol{M} - k_0^2 \boldsymbol{I})\, \vec{e} = \vec{r}\,' \tag{9}$$

with $\boldsymbol{I}$ being the matrix of unity.

The dimension of the system of linear equations for the electric field $\vec{e}$ is very large. Its matrix consists only of a few diagonals with nonzero elements but does not exhibit special properties. It is not symmetric and, what is even more important, it is not positive definite. Thus, convergence of iterative solution methods is very poor, as shown in Section IV-A. In the next section, therefore, a modified formulation is presented which can extremely improve convergence properties and, consequently, reduce computational time.

III. Introduction of the E-Field Divergence

The convergence behavior when solving (9) numerically depends on the properties of the system matrix $(\boldsymbol{M} - k_0^2 \boldsymbol{I})$. Very important are the following conditions: The matrix should be positive definite and should have a symmetric structure $(\boldsymbol{M}^T = \boldsymbol{M})$. Then, only real eigenvalues occur and each of them is larger than zero. In this case, the matrix would be ideally suited for numerical solvers. Regarding (9), however, it seems to be impossible to proof generally whether the matrix is positive definite or not. One gets further insight, however, when analyzing the internal structure of the system matrix $(\boldsymbol{M} - k_0^2 \boldsymbol{I})$ and relating it to the physical problem (see Weiland [6]).

What one needs to know are the eigenvalues of this matrix, because they determine its numerical condition. The term $-k_0^2 \boldsymbol{I}$ causes only a shift and thus the problem is to derive the eigenvalues λ_i of $\boldsymbol{M}$. The characteristic equation reads

$$\det (\boldsymbol{M} - \lambda_i \boldsymbol{I}) = 0. \tag{10}$$

Comparing this expression to the original problem stated by (9) one finds that the λ_i refer to the resonances of the equivalent cavity. If one treats the case without any sources on the enclosure (i.e., $\vec{r} = 0$ in (9)), each eigenvalue λ_i in (10) corresponds to a resonance frequency with

$k_{0\text{res}} = 2\pi f_{0\text{res}}\sqrt{\epsilon_0\mu_0}$ in (9). In conclusion, the eigenvalues of the system matrix and thus its numerical condition correlate to the cavity resonances of the enclosure. Particularly, if there exists a resonance for $f_{0\text{res}} = 0$ Hz, the system matrix possesses an eigenvalue at zero and hence cannot be positive definite—a case that should be avoided. Our investigations show that it has a severe impact on the numerical procedure and, therefore, further considerations on the solution for $\omega = 0$ are necessary.

From the physical point of view, the situation is clear: When the metallic boundaries and the metallic regions inside the box are simply connected, resonant fields of frequency $f_{0\text{res}} = 0$ Hz can only be generated by an electric space charge ρ in the dielectric areas. $\rho(x, y, z)$ can be arbitrarily distributed because a priori we did not assume any condition on $\nabla \cdot \epsilon\vec{E} = \rho$. The space charge excites an irrotational static field, which is a solution of (9) and (10) and inevitably generates eigenvalues at zero. More detailed, for all n nodes containing only dielectric material an arbitrary charge value is possible. Therefore, at a frequency of zero n independent solutions are possible for resonant fields. Hence a n-times degenerated eigenvalue for the corresponding resonator problem must be expected.

Since we are focusing on time-dependent solutions, static fields including those excited by a static space charge do not influence our solution on principle. As shown above, however, they change the matrix involved in the numerical procedure causing additional eigenvalues at zero, which drastically deteriorate convergence characteristics.

The basic idea, developed already by Weiland for resonator problems [5], is to force the static space charges to zero by imposing the condition of zero space charge (11) on (9) and (8):

$$\nabla \cdot \epsilon\vec{E} = \rho = 0 \triangleq \oint_A \epsilon\vec{E}\, d\vec{A} = 0 \tag{11}$$

Then, assuming simply connected metallic regions inside the box, all resonances at $\omega = 0$ and the corresponding eigenvalues of the system matrix vanish. Condition (11), of course, should only be used for dielectric regions, since charges may exist on *metallic* walls and inlays.

Equation (11) can be transformed into a finite-difference formulation for node m of the mesh as explained in Appendix I. In matrix form it reads

$$\boldsymbol{B}\boldsymbol{D}_{A\epsilon}\,\vec{e} = \vec{0}. \tag{12}$$

The matrix $\boldsymbol{B}$ represents here, similar to matrix $\boldsymbol{A}$, the integral over a closed surface without considering mesh dimensions or material parameters (see Appendix II). These informations are included in the diagonal matrix $\boldsymbol{D}_{A\epsilon}$.

One can rewrite (12) without loosing generality in the following way:

$$(\boldsymbol{D}_s^{-1}\boldsymbol{D}_{A\epsilon}\boldsymbol{B}^T\boldsymbol{D}_{V\epsilon\epsilon}^{-1}\boldsymbol{B}\boldsymbol{D}_{A\epsilon})\,\vec{e} = \vec{0} \tag{13}$$

This equation is equivalent to the operator:

$$\nabla(\nabla \cdot \epsilon\vec{E}) = \vec{0}. \tag{14}$$

One can now incorporate (13) into the basic formulation of (8):

$$(\boldsymbol{A}^T\boldsymbol{D}_{s/\mu}\boldsymbol{D}_A^{-1}\boldsymbol{A}\boldsymbol{D}_s - k_0^2\boldsymbol{D}_{A\epsilon} + \phi\boldsymbol{D}_s^{-1}\boldsymbol{D}_{A\epsilon}\boldsymbol{B}^T\boldsymbol{D}_{V\epsilon\epsilon}^{-1}\boldsymbol{B}\boldsymbol{D}_{A\epsilon})\,\vec{e} = \vec{r}. \tag{15}$$

The factor ϕ is similar to a penalty factor, which does not influence the true solution but can be used to optimize speed of convergence. For all structures investigated ϕ is found to be equal to unity. Therefore, it is omitted in the following equations.

Employing (15) instead of (8) or (9), one can be sure now that for simply connected metallic boundaries and inlays the lowest resonance frequency of the whole structure is not equal to zero.

Also, after some mathematical manipulations the system matrix of (15) can be transformed into a symmetric one:

$$(\boldsymbol{D}_s^{1/2}\boldsymbol{A}^T\boldsymbol{D}_{s/\mu}\boldsymbol{D}_A^{-1}\boldsymbol{A}\boldsymbol{D}_s^{1/2} - k_0^2\boldsymbol{D}_{A\epsilon} + \boldsymbol{D}_s^{-1/2}\boldsymbol{D}_{A\epsilon}\boldsymbol{B}^T\boldsymbol{D}_{V\epsilon\epsilon}^{-1}\boldsymbol{B}\boldsymbol{D}_{A\epsilon}\boldsymbol{D}_s^{-1/2})\boldsymbol{D}_s^{1/2}\,\vec{e} = \boldsymbol{D}_s^{1/2}\,\vec{r}. \tag{16}$$

This linear system of equations can be solved numerically much faster than the original formulation of (8) (see Section IV-A). It is interesting to note that this improvement depends not only on the divergence condition (11) itself. Rather we found that it must be implemented in (9) by the formulation $\nabla(\nabla \cdot \epsilon\vec{E})$ according to (13). Obviously, the new formulation presented in (16) and (15) corresponds to the derivation of the Helmholtz wave equation where also the condition $\nabla(\nabla \cdot \epsilon\vec{E})$ is required to obtain $\nabla^2\vec{E} + k^2\vec{E}$ from the original Maxwell operator $\nabla \times \nabla \times \vec{E} - k^2\vec{E}$.

IV. Results

A. The Numerical Advantage of the New Formulation

Our software package is based on the work by Christ [7], who, however, did not include the above mentioned divergence formulation. It runs on a IBM3090-200VF mainframe computer. For the solution of the larger linear equation system, the mathematical library LINSOL [8] is used. This library contains several iterative solution methods, of which the biconjugate-gradient method (BICO) is selected to solve the large linear equation system.

To demonstrate the advantage of the new formulation, Table I presents some data on the numerical efforts using the new formulation and the standard version without the divergence condition, respectively.

The first structure (MS-DIS) is a microstrip discontinuity where the width of the strip changes. The mesh is nearly equidistant and very coarse, with a relatively small number of nodes, namely 1600. Therefore, the advantage

TABLE I
COMPARISON OF THE NEW FINITE-DIFFERENCE FORMULATION CONSIDERING $\nabla \cdot \epsilon\vec{E} = 0$ WITH THE STANDARD VERSION, IN TERMS OF MATRIX-VECTOR MULTIPLICATIONS (NO. MVM) AND CPU TIME IN SECONDS

	Computational Efforts			
Structure	No. MVM	CPU Time	No. MVM	CPU time
	Standard Version		With $\nabla \cdot \epsilon\vec{E} = 0$	
MS-DIS	1996	11	264	2
AB-A-L10-11	58204	4756	1416	118

of the new formulation is considerable (a factor of 6 in CPU time) but not as extreme as for the second case. The latter structure, an air-bridge for coplanar MMIC's, requires a strongly nonequidistant mesh (ratio between the cell dimensions up to 27) consisting of 6630 nodes and, correspondingly, shows a very poor convergence for the standard version. For this geometry, the reduction in CPU time reaches a factor of 40.

This improvement is a very essential one regarding application of the FD method to the typical three-dimensional problems encountered in the analysis of MMIC elements. Coplanar discontinuities, for instance, require a strongly non-equidistant mesh due to their inhomogeneous field distribution. The mesh has to be very fine in the slot area and successively coarse towards the shielding. For such problems, the formulation without considering $\nabla \cdot \epsilon\vec{E} = 0$ leads to an extremely poor convergence or even divergence of the equation solver. Thus the improved formulation presented here actually opens new fields of application.

B. Comparison with Other Methods

In order to show the stability and accuracy of our finite-difference formulation, the scattering parameters (more precisely, $|S_{11}|$ and $\phi_{21} = \arg(S_{21})$) of a microstrip meander transmission-line are plotted in Figs. 2 and 3. The results obtained by measurements (solid line) [9] and by two other field simulation techniques are shown as well. One of them uses the spectral domain approach (SDA) (dashed line) [10] while the other data (dotted line) refer to a finite-difference formulation in time domain (FDTD) [4].

Generally, the agreement between measurements and predicted results is good. For high frequencies ($f > 22$ GHz), a box resonance must be taken into account, which causes the difference between our results (bullet) and the other field simulation techniques. It should be pointed out, that one finds a particular good agreement between the two finite-difference formulations. The shift of $|S_{11}|$ in the frequency range from 14 GHz up to 22 GHz is caused by radiation losses that are included in the time domain case due to the open boundary condition. As already mentioned in [4], for a finite-difference formulation in time domain a frequency shift of the scattering parameters can be observed. Presumably, this error is caused by an inaccurate description of the metallization dimensions due to the discretized formulation [11]. The FDTD seems to enlarge the metallization by a small extent, i.e., the results correspond to a structure with metallic inlays, which are slightly larger than the actual ones. It can be seen from our investigations, that this error also occur in the frequency-domain formulation. A reduction of the error is possible using a finer mesh, which, however, increases the dimension of the system matrix.

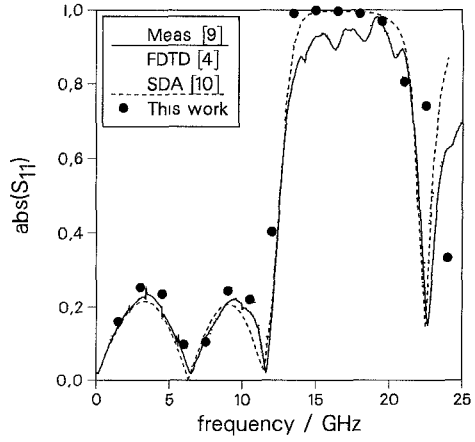

Fig. 2. $|S_{11}|$ of a microstrip meander transmission-line.

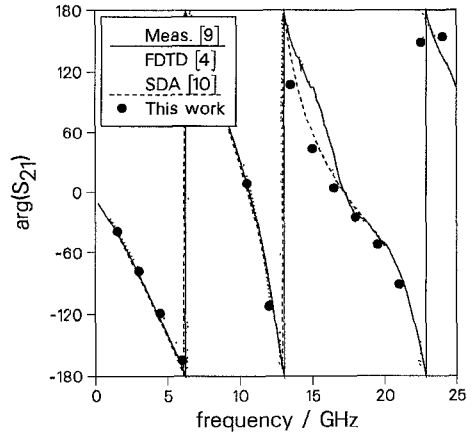

Fig. 3. arg $(S_{21}) = \phi_{21}$ of a microstrip meander transmission-line.

In Fig. 4, the effective length l_{eff} of an open microstrip end is shown in comparison to previous work [12]–[14] using spectral domain techniques. The frequency dependence agrees very favorably. The effective length, on the other hand, is always about 8% higher than the results obtained by the other methods. This again corresponds to the case of a slightly larger metallization.

The deviations between the references and the lack of accurate measurements, however, make a detailed quantitative comparison impossible.

V. CONCLUSION

The finite-difference method in the frequency domain proved to be a powerful technique for the full-wave analysis of 3-dimensional structures of arbitrary geometry.

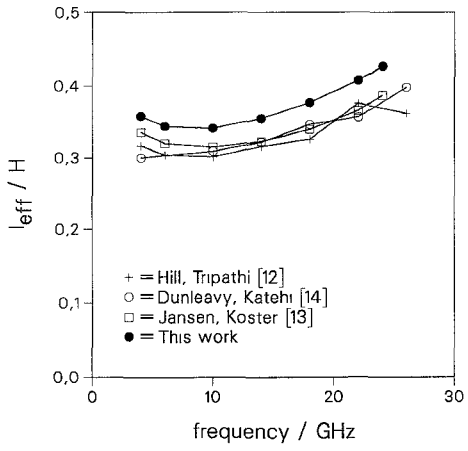

Fig. 4. Effective length l_{eff} of an open microstrip end (H = 0.635 mm, ϵ_r = 9.6 W/H = 1.57).

Explicitly incorporating the E-field divergence, a better numerical convergence behaviour in solving the large system of equations can be achieved. CPU time reductions up to a factor >40 were observed. This enables one to investigate also structures with highly complex geometries, which otherwise could not be analyzed because convergence of the iterative system solver would fail.

Checking the method against previous work on microstrip discontinuities generally good agreement was found. A small systematic error regarding the dimensions of metallic inlays is observed. It appears to be inherent to all finite-difference formulations and results in a slight shift of the scattering parameters towards lower frequencies.

Appendix I

This section describes the transformation of the two Maxwell-equations into a finite-difference formulation in the frequency domain. Regarding the dimensions of each cell and the filling material the following index notation is used. The node corresponding to cell m is that of the left lower front corner. The neighboring cells are denoted by their location regarding to m ((l)eft, (r)ight, (d)own, (u)p, in (f)ront of, (b)ehind). Then (17)–(19) represent the first Maxwell equation (see (1)), while (20)–(22) originate from the second Maxwell equation (see (2)):

$$\frac{1}{2}\left(\frac{z_f}{\mu_f}+\frac{z_m}{\mu_m}\right)B_{zm}-\frac{1}{2}\left(\frac{y_m}{\mu_m}+\frac{y_l}{\mu_l}\right)B_{ym}-\frac{1}{2}\left(\frac{z_l}{\mu_l}+\frac{z_{lf}}{\mu_{lf}}\right)B_{zl}+\frac{1}{2}\left(\frac{y_{lf}}{\mu_{lf}}+\frac{y_f}{\mu_f}\right)B_{yf}=j\omega\epsilon_0\mu_0\left(\frac{y_m z_m}{4}\epsilon_m+\frac{z_l y_l}{4}\epsilon_l+\frac{y_{lf}z_{lf}}{4}\epsilon_{lf}+\frac{z_f y_f}{4}\epsilon_f\right)E_{xm} \quad (17)$$

$$\frac{1}{2}\left(\frac{x_d}{\mu_d}+\frac{x_m}{\mu_m}\right)B_{xm}-\frac{1}{2}\left(\frac{z_m}{\mu_m}+\frac{z_f}{\mu_f}\right)B_{zm}-\frac{1}{2}\left(\frac{x_f}{\mu_f}+\frac{x_{df}}{\mu_{df}}\right)B_{xf}+\frac{1}{2}\left(\frac{z_{df}}{\mu_{df}}+\frac{z_d}{\mu_d}\right)B_{zd}=j\omega\epsilon_0\mu_0\left(\frac{z_m x_m}{4}\epsilon_m+\frac{x_f z_f}{4}\epsilon_f+\frac{z_{df}x_{df}}{4}\epsilon_{df}+\frac{x_d z_d}{4}\epsilon_d\right)E_{ym} \quad (18)$$

$$\frac{1}{2}\left(\frac{y_l}{\mu_l}+\frac{y_m}{\mu_m}\right)B_{ym}-\frac{1}{2}\left(\frac{x_m}{\mu_m}+\frac{x_d}{\mu_d}\right)B_{xm}-\frac{1}{2}\left(\frac{y_d}{\mu_d}+\frac{y_{dl}}{\mu_{dl}}\right)B_{yd}+\frac{1}{2}\left(\frac{x_{dl}}{\mu_{dl}}+\frac{x_l}{\mu_l}\right)B_{xl}=j\omega\epsilon_0\mu_0\left(\frac{x_m y_m}{4}\epsilon_m+\frac{y_d x_d}{4}\epsilon_d+\frac{x_{dl}y_{dl}}{4}\epsilon_{dl}+\frac{y_l x_l}{4}\epsilon_l\right)E_{zm} \quad (19)$$

$$z_r E_{zr}-y_b E_{yb}-z_m E_{zm}+y_m E_{ym}=-j\omega y_m z_m B_{xm} \quad (20)$$

$$x_b E_{xb}-z_u E_{zu}-x_m E_{xm}+z_m E_{zm}=-j\omega z_m x_m B_{ym} \quad (21)$$

$$y_u E_{yu}-x_r E_{xr}-y_m E_{ym}+x_m E_{xm}=-j\omega x_m y_m B_{zm}. \quad (22)$$

The additional constraint of the field $\nabla\cdot\epsilon_r\vec{E}=0$ can be transformed into the finite-difference scheme in the following way. Again, the equation refers to grid node m:

$$+\left(\frac{y_m z_m}{4}\epsilon_m+\frac{z_l y_l}{4}\epsilon_l+\frac{y_{lf}z_{lf}}{4}\epsilon_{lf}+\frac{z_f y_f}{4}\epsilon_f\right)E_{xm}-\left(\frac{y_d z_d}{4}\epsilon_d+\frac{z_{dl}y_{dl}}{4}\epsilon_{dl}+\frac{y_{dlf}z_{dlf}}{4}\epsilon_{dlf}+\frac{z_{df}y_{df}}{4}\epsilon_{df}\right)E_{xd}+\left(\frac{z_m x_m}{4}\epsilon_m+\frac{x_f z_f}{4}\epsilon_f+\frac{z_{df}x_{df}}{4}\epsilon_{df}+\frac{x_d z_d}{4}\epsilon_d\right)E_{ym}-\left(\frac{z_l x_l}{4}\epsilon_l+\frac{x_{lf}z_{lf}}{4}\epsilon_{lf}+\frac{z_{dlf}x_{dlf}}{4}\epsilon_{dlf}+\frac{x_{dl}z_{dl}}{4}\epsilon_{dl}\right)E_{yl}+\left(\frac{x_m y_m}{4}\epsilon_m+\frac{y_d x_d}{4}\epsilon_d+\frac{x_{dl}y_{dl}}{4}\epsilon_{dl}+\frac{y_l x_l}{4}\epsilon_l\right)E_{zm}-\left(\frac{x_f y_f}{4}\epsilon_f+\frac{y_{df}x_{df}}{4}\epsilon_{df}+\frac{x_{dlf}y_{dlf}}{4}\epsilon_{dlf}+\frac{y_{lf}x_{lf}}{4}\epsilon_{lf}\right)E_{zf}=0. \quad (23)$$

Appendix II

This section provides information on the morphological structure of the matrices which are used in the description above.

The electric field vector and the magnetic field vector are built up according to (24) and (25):

$$\vec{e}=(\cdots, E_{zm}, E_{ym}, E_{xm}, \cdots) \quad (24)$$

$$\vec{b}=(\cdots, B_{zm}, B_{ym}, B_{xm}, \cdots). \quad (25)$$

The total number of cells is $m_{ges} = n_x \cdot n_y \cdot n_z$ with n_v corresponding to the number of mesh lines in direction v.

The matrix $\boldsymbol{A}$ representing the operator for the integral along a closed line is shown in (26). This matrix consists only of the elements -1, 0 and 1. If one electric component is equal to zero because of its position on a metallic boundary or inlay, the whole column becomes zero. Hence there holds $\det(\boldsymbol{A}) = 0$. The indices u, r, b refer to the position of the corresponding cell related to cell m (see Appendix I):

$$\boldsymbol{A} = \begin{array}{c} \begin{array}{cccccccccccccc} \cdots & zm & ym & xm & zu & yu & \cdots & zr & yr & xr & \cdots & zb & yb & xb & \cdots \end{array} \\ \left[\begin{array}{cccccccccccccc} \ddots & & & & & & & & & & & & & & \\ & 0 & -1 & 1 & 0 & 1 & \cdots & 0 & 0 & -1 & \cdots & 0 & 0 & 0 & \\ & 1 & 0 & -1 & -1 & 0 & \cdots & 0 & 0 & 0 & \cdots & 0 & 0 & 1 & \\ & -1 & 1 & 0 & 0 & 0 & \cdots & 1 & 0 & 0 & \cdots & 0 & -1 & 0 & \\ & & & & 0 & & & & & & & & & & \\ & & & & & 0 & & & & & & & & & \\ & & & & & & \ddots & & & & & & & & \\ & & & & & & & 0 & & & & & & & \\ & & & & & & & & 0 & & & & & & \\ & & & & & & & & & 0 & & & & & \\ & & & & & & & & & & \ddots & & & & \\ & & & & & & & & & & & 0 & & & \\ & & & & & & & & & & & & 0 & & \\ & & & & & & & & & & & & & 0 & \\ & & & & & & & & & & & & & & \ddots \end{array}\right] \end{array} . \tag{26}$$

Matrix $\boldsymbol{B}$ describes a volume integral. This integral can be obtained for every grid node except those who are part of a metallic boundary or inlay. Hence for the whole structure only m_{ges} equations of $\nabla \cdot \epsilon \vec{E} = 0$ are possible. In order to obtain a more homogeneous structure of the matrix, the same equation is considered three times, for the E_{xm}, E_{ym} and E_{zm} components:

$$\boldsymbol{B} = \begin{array}{c} \begin{array}{cccccccccc} \cdots & zf & \cdots & yl & \cdots & xd & zm & ym & xm & \cdots \end{array} \\ \left[\begin{array}{cccccccccc} \ddots & & & & & & & & & \\ & 1 & & & & & & & & \\ & & \ddots & & & & & & & \\ & & & 1 & & & & & & \\ & & & & \ddots & & & & & \\ & & & & & 1 & & & & \\ & -1 & \cdots & -1 & \cdots & -1 & 1 & 1 & 1 & \\ & -1 & \cdots & -1 & \cdots & -1 & 1 & 1 & 1 & \\ & -1 & \cdots & -1 & \cdots & -1 & 1 & 1 & 1 & \\ & & & & & & & & & \ddots \end{array}\right] \end{array} . \tag{27}$$

Finally, the diagonal matrices $\boldsymbol{D}$ containing the information on all dimensions and materials are presented. All cell dimensions are described by their direction with regard to the coordinate system (see Fig. 1) and by an index, which refers to the cell number. This index also characterizes permeability and permittivity of each elementary cell:

$$\boldsymbol{D}_s = \text{Diag}\,(\cdots, z_m, y_m, x_m, \cdots) \tag{28}$$

$$\boldsymbol{D}_A = \text{Diag}\,(\cdots, x_m y_m, x_m z_m, y_m z_m, \cdots) \tag{29}$$

$$\boldsymbol{D}_{s/\mu} = \text{Diag}\left(\cdots, \frac{1}{2}\left(\frac{z_f}{\mu_f} + \frac{z_m}{\mu_m}\right), \frac{1}{2}\left(\frac{y_l}{\mu_l} + \frac{y_m}{\mu_m}\right), \frac{1}{2}\left(\frac{x_u}{\mu_u} + \frac{x_m}{\mu_m}\right), \cdots\right) \tag{30}$$

$$\boldsymbol{D}_{A\epsilon} = \text{Diag}\left(\cdots, \frac{1}{4}(x_m y_m \epsilon_m + y_d x_d \epsilon_d + x_{dl} y_{dl} \epsilon_{dl} + y_l x_l \epsilon_l), \frac{1}{4}(z_m x_m \epsilon_m + x_f z_f \epsilon_f + z_{df} x_{df} \epsilon_{df} + x_d z_d \epsilon_d), \frac{1}{4}(y_m z_m \epsilon_m + z_l y_l \epsilon_l + y_{lf} z_{lf} \epsilon_{lf} + z_f y_f \epsilon_f), \cdots\right) \tag{31}$$

$$\boldsymbol{D}_{V\epsilon\epsilon} = \text{Diag}(\cdots, d_{V\epsilon\epsilon m}, d_{V\epsilon\epsilon m}, \cdots)$$

$$d_{V\epsilon\epsilon m} = \frac{1}{8}(z_{dlf} y_{dlf} x_{dlf} \epsilon_{dlf}^2 + z_{lf} y_{lf} x_{lf} \epsilon_{lf}^2 + z_{df} y_{df} x_{df} \epsilon_{lf}^2 + z_f y_f x_f \epsilon_f^2 + z_{dl} y_{dl} x_{dl} \epsilon_{dl}^2 + z_l y_l x_l \epsilon_l^2 + z_d y_d x_d \epsilon_d^2 + z_m y_m x_m \epsilon_m^2). \tag{32}$$

References

[1] T. Hirota, K. Honjo, and H. Ogawa, "Uniplanar MMIC hybrids—A proposed new MMIC structure," *IEEE Trans. Microwave Theory Tech.*, vol. MTT-35, pp. 576–581, June 1987.

[2] H. Katzier, "Streuverhalten elektromagnetischer Wellen bei sprunghaften Übergängen geschirmter dielektrischer Leitungen," *Arch. Elek. Übertragung.*, vol. 38, pp. 290–296, 1984.

[3] N. H. L. Koster and R. H. Jansen, "The microstrip step discontinuity: A revised description," *IEEE Trans. Microwave Theory Tech.*, vol. MTT-34, pp. 213–223, Feb. 1987.

[4] M. Rittweger and I. Wolff, "Analysis of complex passive (M)MIC-components using the finite difference time-domain approach," in *1990 IEEE MTT-S Int. Microwave Symp. Dig.*, pp. 1147–1150.

[5] T. Weiland, "Three dimensional resonator mode computation by finite difference method," *IEEE Trans. Magn.*, vol. MAG-21, pp. 2340–2343, Nov. 1985.

[6] ——, "On the unique numerical solution of Maxwell eigenvalue problems in three dimensions," *Particle Accelerators*, vol. 17, pp. 227–242, 1985.

[7] A. Christ and H. L. Hartnagel, "Three-Dimensional Finite-Difference Method for the Analysis of Microwave-Device Embedding," *IEEE Trans. Microwave Theory Tech.*, vol. MTT-35, pp. 688–696, Aug. 1987.

[8] H. Müller, W. Schönauer, and E. Schnepf, "Design considerations for the linear solver LINSOL on a CYBER 205," *Super-Computer Applications*, A. H. L. Emmen, Ed. New York: North Holland, 1985, pp. 39–49.

[9] G. Gronau and M. Rittweger, "*S*-parameter measurements on microstrip meander line," private communication, Duisburg 1991.

[10] W. Wertgen and R. H. Jansen, "Efficient direct and iterative electrodynamic analysis of geometrically complex MIC and MMIC structures," *Int. J. Numerical Modelling*, vol. 2, pp. 153–186, 1989.

[11] C. J. Railton and J. P. McGeehan, "Analysis of microstrip discontinuities using the finite difference time domain technique," in *1989 IEEE MTT-S Int. Microwave Symp. Dig.*, pp. 1009–1012.

[12] A. Hill and V. K. Tripathi, "An efficient algorithm for the three-dimensional analysis of passive microstrip components and discontinuities for microwave and millimeter-wave integrated circuits," *IEEE Trans. Microwave Theory Tech.*, vol. 39, pp. 83–91, Jan. 1991.

[13] R. H. Jansen and N. H. L. Koster, "Accurate results on the end effect of single and coupled microstrip lines for use in microwave circuit design," *Arch. Elek. Übertragung.*, vol. 34, pp. 453–459, 1980.

[14] L. P. Dunleavy and P. B. Katehi, "Shielding effects in microstrip discontinuities," *IEEE Trans. Microwave Theory Tech.*, vol. 36, pp. 1767–1774, Dec. 1988.

Klaus Beilenhoff (M'90) was born in Soest, Germany, in 1963. He received the Dipl.-Ing. degree in electrical engineering from the Technical University of Darmstadt, Germany, in 1989.

Since then he has been working at the Institut für Hochfrequenztechnik of the Technical University of Darmstadt, where he is engaged in numerical computation of electromagnetic fields applied to MMIC structures.

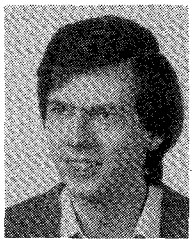

Wolfgang Heinrich (M'84) was born in Frankfurt, Germany, in 1958. He received the Dipl.-Ing. and Dr.-Ing. degrees in 1982 and 1987, respectively, both from the Technical University of Darmstadt, Germany.

In 1983, he joined the staff of the Institut für Hochfrequenztechnik of the Technical University of Darmstadt, where he is currently engaged in field-theoretical work on planar transmission lines.

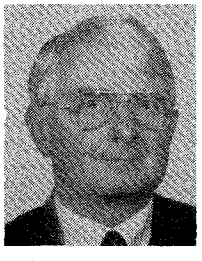

Hans L. Hartnagel (SM'72) was born in Geldern, Germany, in 1934. He received the Dipl.Ing. degree in 1960 from the Technical University Aachen, Germany, and the Ph.D. and the Dr.Eng. degrees from the University of Sheffield, England, in 1964 and 1971, respectively.

After having worked for a short period with the company Telefunken in Ulm, Germany, he joined the Institut National des Sciences Appliquées, Villeurbanne, Rhône, France. He then joined the Department of Electronic and Electrical Engineering of the University of Sheffield, in 1962 first as a Senior Research Assistant, then as a Lecturer and later on as a Senior Lecturer and Reader. In January 1971 he held the position of Professor of Electronic Engineering at the University of Newcastle upon Tyne, in England. Since October 1978 he has been the Professor of High Frequency Electronics at the Technical University of Darmstadt in Germany.

Dr. Hartnagel is the author of books and numerous scientific papers, originally on microwave tubes and later on concerning microwave semiconductor devices, their technology and their circuits. He has held many consulting positions, partly while on temporary leave of absence from his University positions.